ACSNANO
www.acsnano.org
ARTICLE

Transient Nanoscopic Phase Separation in Biological Lipid Membranes Resolved by Planar Plasmonic Antennas

Pamina M. Winkler,[†] Raju Regmi,[‡,†] Valentin Flauraud,[§] Jürgen Brugger,[§] Hervé Rigneault,[‡] Jérôme Wenger,[*,‡] and María F. García-Parajo[*,†,⊥]

[†]Institut de Ciencies Fotoniques (ICFO), The Barcelona Institute of Science and Technology, Barcelona, Spain
[‡]Aix Marseille Univ, CNRS, Centrale Marseille, Institut Fresnel, Marseille, France
[§]Microsystems Laboratory, Institute of Microengineering, Ecole Polytechnique Fédérale de Lausanne, 1015 Lausanne, Switzerland
[⊥]ICREA, Pg. Lluís Companys 23, 08010 Barcelona, Spain

Supporting Information

ABSTRACT: **Nanoscale membrane assemblies of sphingolipids, cholesterol, and certain proteins, also known as lipid rafts, play a crucial role in facilitating a broad range of important cell functions. Whereas on living cell membranes lipid rafts have been postulated to have nanoscopic dimensions and to be highly transient, the existence of a similar type of dynamic nanodomains in multicomponent lipid bilayers has been questioned. Here, we perform fluorescence correlation spectroscopy on planar plasmonic antenna arrays with different nanogap sizes to assess the dynamic nanoscale organization of mimetic biological membranes. Our approach takes advantage of the highly enhanced and confined excitation light provided by the nanoantennas together with their outstanding planarity to investigate membrane regions as small as 10 nm in size with microsecond time resolution. Our diffusion data are consistent with the coexistence of transient nanoscopic domains in both the liquid-ordered and the liquid-disordered microscopic phases of multicomponent lipid bilayers. These nanodomains have characteristic residence times between 30 and 150 μs and sizes around 10 nm, as inferred from the diffusion data. Thus, although microscale phase separation occurs on mimetic membranes, nanoscopic domains also coexist, suggesting that these transient assemblies might be similar to those occurring in living cells, which in the absence of raft-stabilizing proteins are poised to be short-lived. Importantly, our work underscores the high potential of photonic nanoantennas to interrogate the nanoscale heterogeneity of native biological membranes with ultrahigh spatiotemporal resolution.**

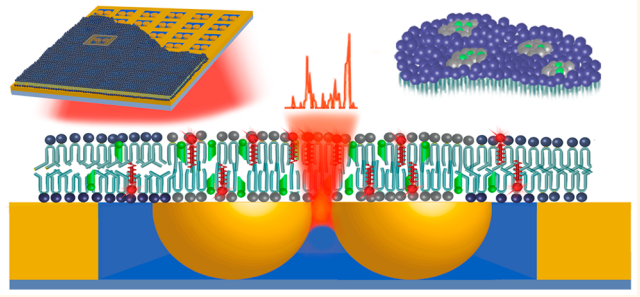

KEYWORDS: *optical nanoantennas, fluorescence correlation spectroscopy, FCS diffusion laws, biological membranes, lipid rafts*

The spatiotemporal lateral organization and the biological function of the eukaryotic plasma membrane are intricately interlaced at the nanoscale. It is well accepted that the landscape of the cell membrane is highly heterogeneous and shaped by a variety of lipids and proteins that differ in their physicochemical properties. In the plane of the membrane, lateral heterogeneities resulting from the formation of specialized regions enriched in sphingolipids, cholesterol, and specific proteins are commonly known as lipid rafts.[1−4] These lipid assemblies are thought to constitute a tightly packed, short-range, liquid-ordered (Lo) phase coexisting with a more liquid-disordered (Ld) phase within the surrounding fluid membrane.[5−7] While the existence of phase separation in the plasma membrane has been debated for many years, a large number of recent experimental data convincingly demonstrates that lipid rafts in living cell membranes have nanoscopic dimensions and are highly dynamic.[8−13] Importantly, lipid rafts play a crucial role in many cellular processes that include signal transduction, protein and lipid sorting, and immune response among others.[2,5,10,14,15] Understanding the formation mechanism and properties (*e.g.*, size, composition) of lipid rafts and relating their structure to their functional role are of paramount interest.

Model lipid membranes represent a simple mimetic system that recapitulates some of the most important features of

Received: May 8, 2017
Accepted: July 11, 2017
Published: July 11, 2017

DOI: 10.1021/acsnano.7b03177
ACS Nano 2017, 11, 7241−7250

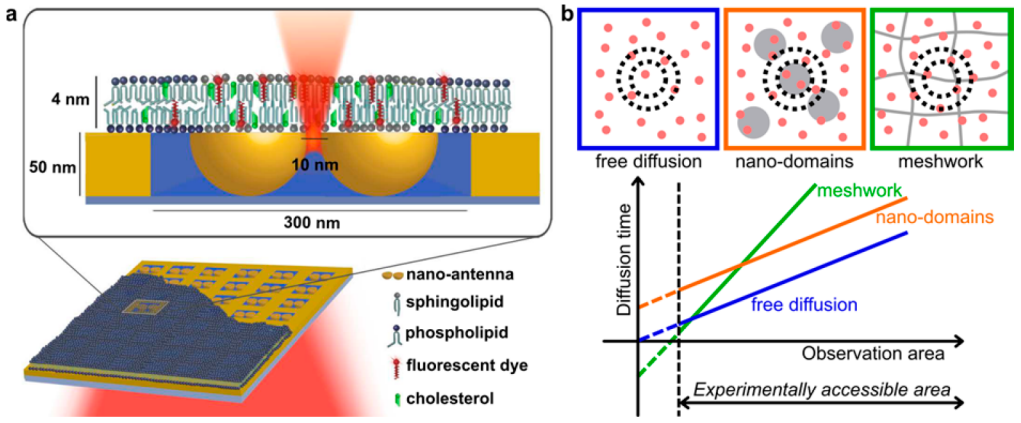

Figure 1. Biological lipid membranes probed by *in-plane* plasmonic antenna arrays. (a) Schematics of the experimental measurements. Bilayers of different lipid compositions are deposited on top of *in-plane* antenna arrays. Each antenna consists of a gold dimer separated by a nanogap and embedded in a nanoaperture. Individual antennas are excited using a confocal setup. The confined and enhanced field at the antenna hotspot excites individual DiD molecules embedded in the bilayer. Fluorescence fluctuations arising from the passage of molecules through the hotpot of the antenna are recorded and autocorrelated in time to generate ACF curves. (b) FCS diffusion laws to extract the type of diffusion exhibited by molecules in biological membranes. The excitation area (dashed circles in the upper sketch) is varied, and the diffusion time of molecules (red dots) is plotted as a function of the excitation area (lower plot). The vertical dashed line in the plot denotes the experimentally accessible area. Three different plots can be obtained reflecting the type of diffusion experienced by the molecule. Continuous lines represent measured values on the experimentally accessible illumination areas. Dashed lines correspond to the extrapolation of the curves through the *y*-intercept. The plots are fitted to $\tau(\omega^2) = t_0 + \omega^2/(4 \times D)$, where ω^2 corresponds to the illumination area, D to the effective diffusion coefficient, and t_0 corresponds to the *y*-intercept. Free diffusion is characterized by $t_0 = 0$; $t_0 > 0$ denotes constrained diffusion due to nanodomains, and $t_0 < 0$ corresponds to constrained diffusion due to meshwork obstacles.

biological membranes, *i.e.*, spatiotemporal compartmentalization and lipid phase separation. On the microscopic scale, ternary lipid membranes composed of unsaturated phospholipids, saturated sphingolipids, and cholesterol separate into coexisting Ld and Lo phases, which can be resolved by diffraction-limited optics.[16−18] The large microscopic size and the stable nature of Lo domains observed on mimetic membranes strongly contrast with the highly transient and nanoscopic size of lipid rafts inferred on living cells. Interestingly, while there is a continuous push for resolving nanoscopic lipid domains in the plasma membranes of living cells, recent works suggest that the microscopically homogeneous Lo and Ld phases on lipid model membranes might in fact also be heterogeneously organized at the nanometer scale.[6,19,20]

The possibility that nanoscale lipid heterogeneities also exist within the supposedly homogeneous Lo and Ld phases of artificial membranes is intriguing and of particular interest as they might be the underlying basis for lipid raft formation in living cells. Indeed, earlier work from Hancock and co-workers predicted that in the absence of stabilizing proteins, the size of lipid nanoassemblies would be smaller than 10 nm in diameter and short-lived, with lifetimes below 1 ms.[6,21] Consistent with this hypothesis, recent deuterium-based nuclear magnetic resonance (d-NMR) experiments revealed the presence of cholesterol and sphingolipids in the Ld phase as well as of unsaturated lipids in the Lo phase, suggesting that nanosized clusters may exist in both phases.[19] Fluorescence correlation spectroscopy (FCS) in combination with stimulated emission depletion (STED) nanoscopy has been recently applied to study the nanoscale dynamics occurring in Lo and Ld phases of ternary lipid-cholesterol mixtures with a spatial resolution of 40 nm. The results showed fully homogeneous Lo and Ld phases with no evidence on the occurrence of nanoscopic domains at the tested spatial scales (40−250 nm).[22] However, it is possible that nanoscale assemblies smaller than the 40 nm STED resolution could not be detected. In contrast to these results, recent high-speed single particle tracking (SPT) of 20 nm gold beads attached to individual lipids showed anomalous diffusion on the Lo phase consistent with the occurrence of nanoscale heterogeneities, while homogeneous lipid diffusion was observed on the Ld phase.[20] The estimated sizes of the nanodomains on the Lo phase varied between 20 to 40 nm with lipid trapping times inside the domains below 1 ms.

A different, and potentially powerful, approach to investigate dynamic nanoscale heterogeneities of lipid bilayers is provided by the use of plasmonic antennas. These metal nanostructures enhance and confine light down to nanoscale dimensions, sustaining localized hotspot regions of the excitation light.[23−26] Moreover, when combined with FCS, single-molecule detection at ultrahigh sample concentrations with microsecond time resolution can be obtained, both in solution and living cell membranes.[27−31] However, in most antenna designs the region of maximum field localization and enhancement (*i.e.*, hotspot) is buried into the nanostructure and thus difficult to access. Recently, we overcame this drawback by fabricating *in-plane* dimer antenna arrays where the gap region is located at the sample surface.[32] This design provides direct accessibility to the antenna hotspot region and drastically improves the optical performance to yield fluorescence enhancement factors of up to 10^4−10^5 together with nanoscale detection volumes in the zeptoliter range.[32] Here, we take advantage of the strong optical confinement occurring on plasmonic antenna arrays together with their remarkable planarity to inquire on the nanoscale dynamics of multicomponent lipid bilayers. Our results reveal the coexistence of transient nanoscopic domains in both the Lo and Ld phase, in the microsecond scale and with characteristic sizes below 10 nm. These nanoscale assemblies might be reminiscent to those naturally occurring in living cells, which in the absence of raft-stabilizing proteins, are expected to be highly transient.

DOI: 10.1021/acsnano.7b03177
ACS Nano 2017, 11, 7241−7250

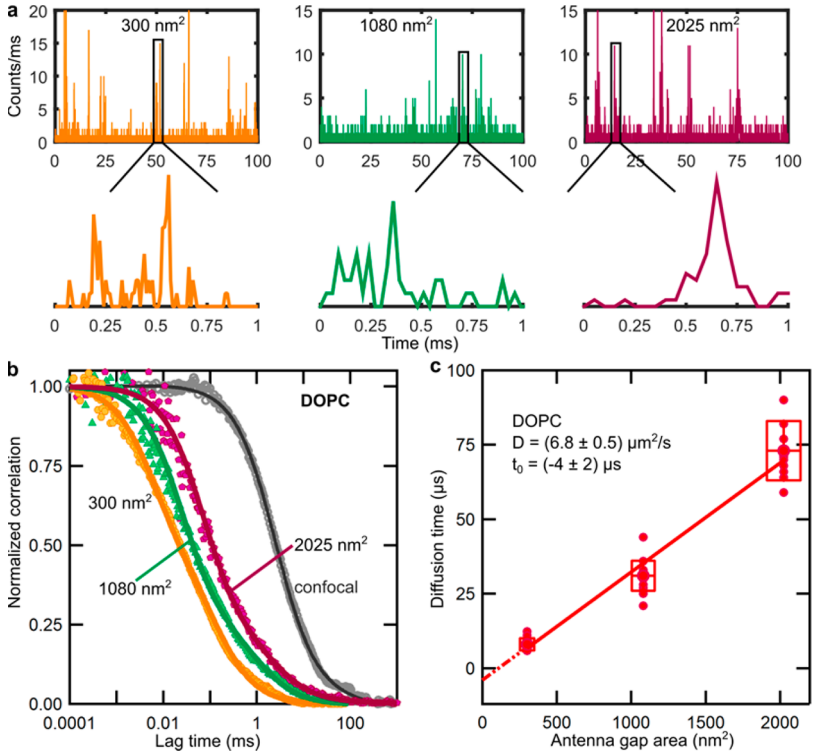

Figure 2. FCS measurements in pure DOPC bilayers using *in-plane* plasmonic antenna arrays of different gap sizes. (a) Representative fluorescence intensity time traces of DiD embedded in a pure DOPC bilayer for three different antenna gap areas together with enlarged views of representative bursts. (b) Normalized ACF curves as obtained from different antenna gap areas and by confocal excitation. (c) Diffusion times as extracted from the ACF fitting as a function of the antenna gap area. Each dot corresponds to an individual ACF measurement in a single antenna. Number of measurements: 13, 8, and 12 for antenna gap areas of 300, 1080, and 2025 nm^2, respectively, on five different samples. Fitting by orthogonal distance regression (red line) has been performed through the mean diffusion time values of each respective antenna gap area minimizing the error for the gap area and ±1std in diffusion time (horizontal and vertical line of the red box, respectively).

RESULTS AND DISCUSSION

Model lipid bilayers with different compositions were prepared on glass coverslips or on top of antenna substrates following a modified protocol from ref 33 and explained in the Methods section. Bilayers were composed of the unsaturated phospholipid 1,2-dioleoyl-*sn*-glycerol-3-phosphocholine (DOPC) alone, DOPC in combination with sphingomyelin (18:0 SM) (1:1 molar proportions) and of ternary mixtures of DOPC, SM (1:1) with addition of 10 or 20 mol % cholesterol (Chol). The different bilayers were labeled with the lipophilic fluorescent dye DiD which preferentially partitions in the Ld phase.[34,35] The quality of the glass-supported bilayers was assessed by FCS measurements using a diffraction-limited confocal microscope. The obtained diffusion values are in good quantitative agreement with values reported for similar lipid mixtures[34] (see Supporting Information Figure S1, Table S1, and related discussion).

To investigate the existence of nanoscale heterogeneities in the different lipid mixtures, we used the same preparation protocol to create bilayers on top of the in-plane antenna substrates as schematically illustrated in Figure 1a. The antenna design consisted of gold dimers of 80 nm in diameter separated by nanogaps of different sizes (from 10 to 45 nm) and surrounded by nanoapertures to further constrain the excitation area and reduce background contribution from fluorescent molecules diffusing outside the antenna hotspots (Supporting Information Figure S2a).[32] For the experiments reported here, we took advantage of the *in-plane* antenna geometry to have access to the maximum spatial confinement at the gap regions. In addition, considering that the height difference between the gold dimers and the filling polymer at the hotspot measurement site is below 3 nm (Supporting Information Figure S2b), we regard these substrates as of excellent planarity and thus suitable for membrane studies.

FCS is a single-molecule sensitive technique that records intensity fluctuations of fluorophores as they transit through the illumination volume. The obtained intensity fluctuations are temporally correlated, and the resulting autocorrelation function (ACF) provides quantitative information on the diffusion behavior and absolute concentration of the detected molecules. To assess the presence of nanoscale heterogeneities in the lipid membranes that would alter the diffusion of the dye, we carried out FCS experiments on antennas of different gap sizes to record the evolution of the diffusion time as a function of the illumination area. This approach exploits the so-called FCS diffusion laws as introduced in ref 36. A diffusion law or diffusion plot is a curve representing the progression of the molecular diffusion time for increasing detection areas, which generally follows a straight line (Figure 1b). The slope of the curve represents the effective diffusion coefficient describing the long-range mobility of the molecule, while the *y*-intercept t_0 on the time axis indicates whether the molecule undergoes free Brownian diffusion ($t_0 = 0$) or is dynamically partitioning into nanodomains ($t_0 > 0$) or trapped in a molecular meshwork ($t_0 < 0$).[36,37]

In this work, we used nanoantennas of nominally 10, 30, and 45 nm gap sizes. The sizes of the illumination areas were estimated based on the gap sizes as measured on TEM images

DOI: 10.1021/acsnano.7b03177
ACS Nano 2017, 11, 7241−7250

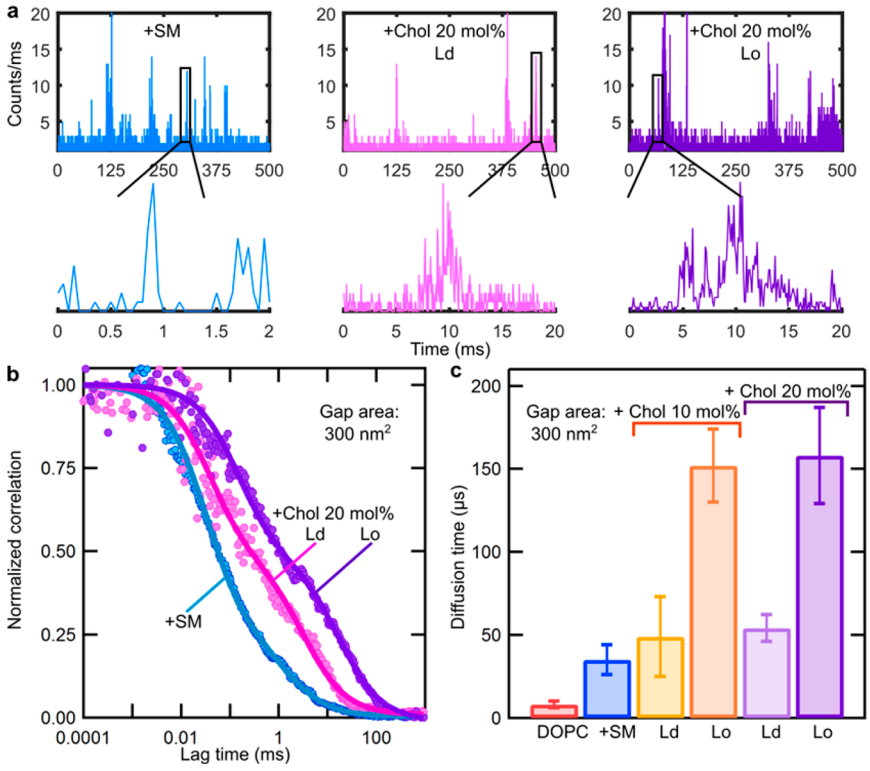

Figure 3. FCS measurements recorded in nanogaps of 300 nm² area for binary and ternary lipid mixtures. (a) Fluorescence intensity time traces of DiD diffusion in DOPC:SM (1:1) (left, blue) and DOPC:SM (1:1) + Chol (20 mol %) in the Ld (middle, magenta) and Lo (right, purple) phases. Enlarged views of single bursts are also depicted for visual comparison. (b) Normalized ACF curves for the different lipid mixtures. (c) Mean diffusion times of the four probed lipid membranes ±1std obtained for the smallest gap area (300 ± 48) nm². Number of measurements: 20 for DOPC; 19 for DOPC:SM; 18 and 15 for Ld and Lo, respectively, with Chol 10 mol %; and 17 and 15 for Ld and Lo, respectively, with Chol 20 mol %. Between 5 and 10 different antennas of 300 nm² area on 4−5 different samples were used for each lipid composition.

(Supporting Information Figure S3) and numerical simulations (Supporting Information Figure S2c−e and the Methods section). In addition, we performed calibration measurements of the area sizes using the Alexa Fluor 647 dye in solution for five different antenna gap sizes (Supporting Information Figure S4 and the Methods section). From the calibration curves, we experimentally determined values of 300, 1080, and 2025 nm² for the nominal 10, 30, and 45 nm gap antennas, respectively, which are in excellent agreement with the calculated values. The sizes of the illumination areas are between 1 and 2 orders of magnitude smaller than the ones of confocal excitation, underscoring the extreme light confinement afforded by plasmonic antennas.

Samples were excited by focusing the incoming laser light (λ = 640 nm, ~2 kW/cm²) onto individual antennas using a water-immersion objective (NA = 1.2). Under these excitation conditions, the temperature increase at the antenna hotspots due to optical heating was estimated to be only within 1−3 K.[38] The fluorescence signal was collected in reflection mode by the same objective, filtered from the excitation light, and sent to two single photoncounting APD detectors. As the antennas show a polarization-dependent response, we used excitation polarization parallel to the antenna gaps to achieve maximum field enhancement and confinement.[32] Fluorescence fluctuations arising from the diffusion of DiD in the bilayers were recorded for at least 30 s at each individual antenna, and the resulting normalized ACFs were calculated.

Representative fluorescent intensity time traces of DiD diffusion in a pure DOPC membrane over three different antenna gap areas are shown in Figure 2a, together with enlarged views of representative single bursts. The burst duration increases with gap area, confirming that the detected signal arises from the excitation of the dye at the gap regions. This is further substantiated by the normalized ACFs obtained for different gap sizes and compared to confocal measurements (Figure 2b). To extract the diffusion times from individual ACF curves, we performed two-component 2D Brownian fittings to account for both direct excitation from the gap region (≥55−90% of the weighted amplitude) and residual excitation of DiD diffusing through the nanoaperture (see eq 1 in the Methods section). Results of the main component of the fitted curves shown in Figure 2b render τ_{DOPC} values of (6 ± 1) μs, (25 ± 3) μs and (71 ± 25) μs for the respective gap areas of (300, 1080, and 2025) nm² compared to τ_{DOPC} = 3.5 ms for confocal excitation. The complete results of the fittings and relative contributions of the gap and nanoaperture excitation are shown in the Supporting Information Table S2.

Diffusion times obtained from multiple measurements on individual antennas as a function of the probed gap are shown in Figure 2c. The mean values of the diffusion times *versus* gap area could be well-fitted to a straight line with an intercept close to the zero-origin point, indicating that τ_{DOPC} scales linearly with the gap area, consistent with free Brownian diffusion of the dye in the pure DOPC membrane. The slope of the fitting rendered a diffusion coefficient of (6.8 ± 0.5) μm²/s which compares well to our confocal measurements (see Supporting Information Table S1) and values reported elsewhere.[34]

DOI: 10.1021/acsnano.7b03177
ACS Nano 2017, 11, 7241−7250

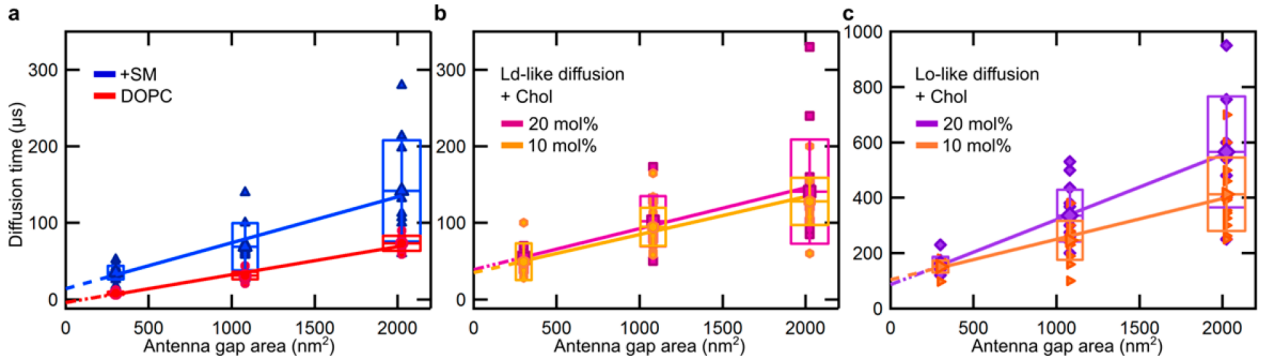

Figure 4. FCS diffusion laws extended to the nanoscale for different lipid mixtures. Diffusion times *versus* antenna gap areas in (a) DOPC and DOPC:SM bilayers. (b) Ld phase for 10 and 20 mol % Chol and (c) Lo phase for 10 and 20 mol % Chol. The colored dots represent diffusion times acquired from FCS on individual nanoantennas of different gap sizes, while the solid lines are fits through the mean values. Measurements were performed on at least 15 different nanoantennas for each lipid composition on 5 different samples.

To further validate that these short diffusion times arise from the strong optical confinement occurring at the surface of the gap regions, we performed experiments on similar antennas with excitation light perpendicular to the antenna gap. In these conditions, the antennas are not resonantly excited, and the excitation field essentially corresponds to that of the surrounding nanoapertures alone. Accordingly, the fluorescence signal is much weaker, and the ACF curves look much noisier (Supporting Information Figure S5). ACF curves for perpendicular excitation could be fitted with a single Brownian diffusion component yielding much longer transient times (1.2−1.9 ms), which are close to the values obtained upon excitation of the nanoaperture alone (*i.e.*, with no antennas inside). These values are also comparable to the t_2 values of the second contribution obtained from the two-component fitting performed on the ACF curves for parallel polarization excitation of the antennas (see also Supporting Information Table S2).

Overall, these results on pure DOPC bilayers validate the application of plasmonic antennas to record the diffusion of individual molecules in lipid bilayers with microsecond time resolution and clearly demonstrate their nanoscale excitation confinement. Additionally, our results show that DOPC bilayers are homogeneous down to the nanoscale. It further confirms that the antenna substrates supporting the bilayers are of extreme flatness and quality, and no hindering effects on the dye diffusion were observed, neither on the DOPC bilayers nor in solution (see also Figure 5a,b).[32] It has been recently reported that molecular pinning and interleaflet membrane coupling effects leading to deviations from free Brownian diffusion at the nanoscale are influenced by the properties of the substrate, *e.g.*, plasma-cleaned glass *versus* mica support.[39] We believe that these effects are not present in our DOPC measurements since: (a) we observed Brownian diffusion of DOPC down to the nanoscale, with a t_0 intercept close to zero; and (b) the gold antenna substrates have been pretreated with UV/ozone plasma cleaning immediately prior to the bilayer deposition (see the Methods section). This treatment leads to a chemically inert and hydrophilic gold surface.[40]

To shed light on the diffusive behavior of lipid membranes composed of binary and ternary mixtures, lipid membranes composed of DOPC:SM (1:1) alone and with the addition of 10 and 20 mol % of Chol were prepared on top of the antenna array substrates and probed by means of FCS. Figure 3a shows characteristic fluorescent intensity time traces of DiD diffusing across the smallest gap antenna (300 nm^2 hotspot area) in DOPC:SM bilayers and on a ternary mixture containing 20 mol % of Chol. In the presence of Chol, stable macroscopic phase separation occurs, so that depending on the antenna location with respect to the membrane, different fluorescence trajectories are recorded, either probing the Ld phase (Figure 3a, middle trajectory) or the Lo phase (Figure 3a, right trajectory). The enlarged views of single bursts of the individual trajectories show increasing burst durations for the binary and ternary mixtures as compared to DOPC (Figure 2a), consistent with slower diffusion of the dye in these lipid mixtures. ACF curves for DOPC:SM and the ternary mixture of DOPC:SM with 20 mol % Chol for both phases (Ld and Lo) are depicted in Figure 3b. As for the DOPC measurements, we fitted all the ACF curves using a two-component 2D Brownian diffusion model. We also attempted to fit the two ACF curves of the ternary mixture to an anomalous diffusion model. However, considering that the anomaly parameter α did not improve the fitting and rendered α values larger than 1, we opted for the use of the two-component 2D Brownian diffusion model. The derived diffusion times at the gap regions for the different lipid compositions resulted in $\tau_{DOPC:SM} = (36 \pm 4)$ μs and $\tau_{Ld} = (39 \pm 9)$ μs and $\tau_{Lo} = (229 \pm 30)$ μs for the 20 mol % Chol ternary lipid mixture. The diffusion times obtained from multiple ACF curves on different 300 nm^2 gap areas for all the different lipid mixtures are summarized in Figure 3c. While DiD in DOPC shows the shortest diffusion time, addition of SM slowed down the dye diffusion consistent with the confocal results. The longest diffusion times were observed for the Lo phase of the ternary mixtures. Interestingly, the diffusion times of DiD in the Ld phase are significantly longer than those obtained in the pure DOPC bilayer, which may already indicate the presence of transient nanoassemblies of Chol in the Ld phase.

To gain more insight into these results, we measured the diffusion times for all the lipid mixtures for different antenna gap sizes and over multiple antennas. The data were fitted through the mean diffusion time values to obtain diffusion laws for each lipid composition (Figure 4). Two main parameters can be directly extracted from the fitting, *i.e.*, the effective diffusion coefficient which is calculated from the slope of the curves and the *y*-intercept of the fitting at zero gap areas (t_0). In the case of DOPC and DOPC:SM bilayers, the intercepts of the fitting cross the origin at nearly zero diffusion times (Figure 4a) consistent with free diffusion of the dye in these lipid bilayers, albeit the diffusion in the DOPC:SM mixture is

DOI: 10.1021/acsnano.7b03177
ACS Nano 2017, 11, 7241−7250

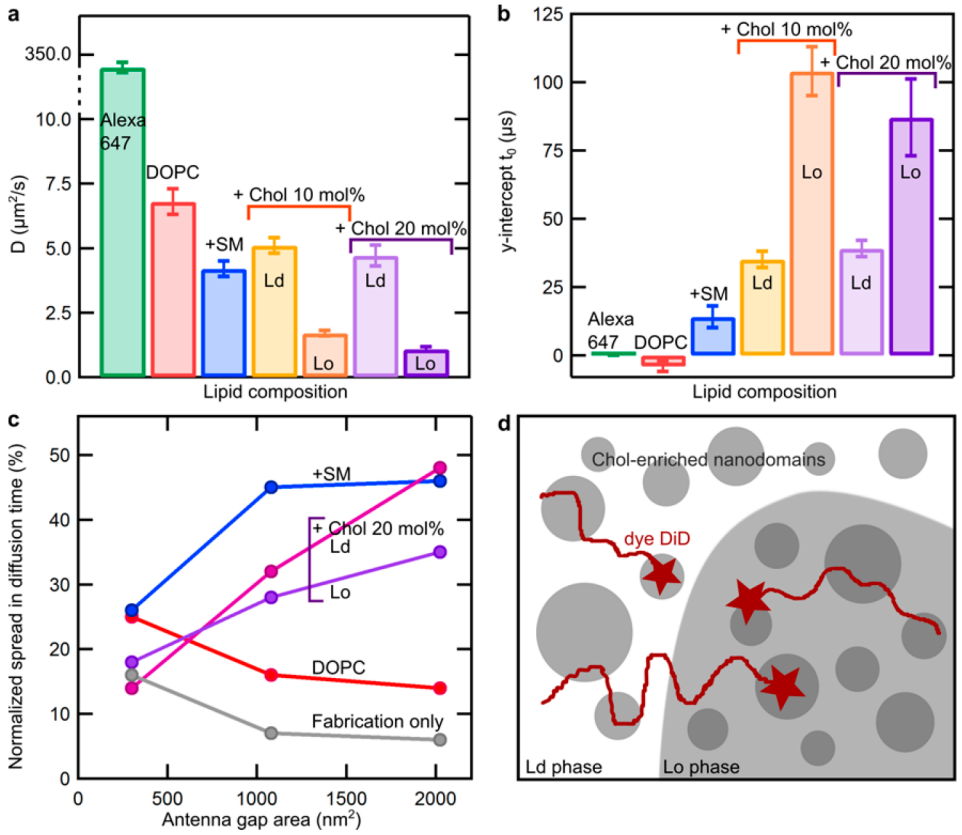

Figure 5. ***In-plane*** **plasmonic nanogap antennas reveal nanoscopic heterogeneities in the Ld and Lo phases of biological lipid membranes. (a) Effective diffusion coefficients** ***D*** **and (b)** ***y*****-intercepts** t_0 **(with ±1std for the errors) as extracted from FCS diffusion laws shown in Figure 4 for the different lipid membrane compositions. Data of the dye Alexa Fluor 647 are included for comparison and show its expected Brownian free diffusion in solution,** ***i.e.,*** $t_0 = 0$ **(taken from ref 32). (c) Normalized spread in diffusion times (±1std/mean ×100%) as a function of the antenna gap area for three different lipid compositions. The gray dots and line correspond to the spread in diffusion times resulting from fabrication inaccuracies of the antenna gaps (variation in gap size/mean gap size, see also Figure S2). (d) Sketch illustrating the presence of dynamic nanoscopic domains inside microscopic Lo and Ld phases of lipid mixtures containing cholesterol.**

significantly slowed down as compared to the pure DOPC membrane due to the tighter packing of saturated SM. In marked contrast, positive t_0 values are obtained for both the Ld and Lo phases in the ternary mixtures containing 10 and 20 mol % Chol, indicating that the diffusion of the dye is not Brownian (Figure 4b,c). Note that the Ld and the Lo phases for the two ternary lipid model membrane mixtures containing 10 and 20 mol % of Chol as shown in Figure 4b,c can clearly be distinguished based on the markedly different diffusion times (see Supporting Information Figure S6).

Results of the effective diffusion coefficients together with the t_0 values for all lipid compositions are shown in Figure 5a,b. For the ternary mixtures containing cholesterol, the diffusion coefficients in the Ld phase are significantly slower than the one of pure DOPC (mean values of 5.1 and 4.7 $\mu m^2/s$ for 10 and 20 mol % Chol, respectively, compared to 6.8 $\mu m^2/s$ for DOPC) (Figure 5a), which is consistent with the longer diffusion times reported in Figure 3c. Moreover, the positive t_0 values indicate a deviation from Brownian diffusion due to the presence of heterogeneities in the Ld phase caused by the occurrence of nanodomains (Figure 5b). These nanoscopic domains are most probably formed by the presence of SM and Chol in the Ld phase, which reduce the effective diffusion of the dye as compared to the pure DOPC bilayer. A similar and even more pronounced trend is also observed in the Lo phase, where the dye experiences very slow effective diffusion and strong deviation from Brownian motion, indicating also the presence of heterogeneities and nanodomains in this phase (Figure 5a,b). Altogether, these results clearly indicate the occurrence of transient nanoscale heterogeneities in both phases of lipid model membranes which have remained so far beyond the detection limits of conventional microscopy.

Further evidence on the heterogeneity within the Lo and Ld phases for ternary lipid bilayers containing Chol can be inferred from the spread of the diffusion times for similar antennas as a function of the gap area, which we quantified as the deviation from the mean diffusion time. Since the metal thin-film morphology affects the fabrication process of the antennas and leads to variations on the real gap areas, we first estimated the spread in diffusion times arising solely from the differences in gap areas (see also Supporting Information, Figure S2). As expected, the spread in diffusion times reduces with increasing gap area as the fabrication process becomes more accurate and smaller variations in the gap sizes are obtained (Figure 5c). In pure DOPC bilayers, DiD shows a spread of the diffusion times that reduces with increasing gap size and essentially reflects the effect of fabrication inaccuracies (Figure 4a and Figure 5c). In striking contrast, the spread of the diffusion times for the binary and ternary compositions increases significantly with gap size (Figure 4a–c and Figure 5c), suggesting the dye samples heterogeneous regions of faster and slower diffusion. These results directly correlate with the positive t_0 values measured,

DOI: 10.1021/acsnano.7b03177
ACS Nano 2017, 11, 7241–7250

indicating the occurrence of heterogeneities in both the Lo and Ld phases due to nanoscopic domains that diffuse through the hotspot gap area during the measurements. Notably, in the case of DOPC:SM, large spreads of the diffusion times are observed for both the (1080 and 2025 nm^2) antennas, although diffusion is largely free and homogeneous (notice that t_0 for the DOPC:SM mixture is slightly positive, *i.e.*, (14 ± 4) μs). We interpret these results as the occurrence of extremely transient local concentrations of SM within the otherwise homogeneous DOPC layer that lead to differences in transient diffusion times but without the occurrence of detectable nanodomains.

The characteristic residence time τ_{res} of the dye in a single nanodomain can be estimated from t_0 through the relation $t_0 \approx 2\alpha\tau_{res}$, since the confinement time is much larger that the free diffusion time inside the domain,[36] and where α corresponds to the partition coefficient of the dye in the Ld and Lo phases.[36] In the case of DiD, the values of α correspond to 0.66 for the Ld phase and 0.33 for the Lo phase evaluated for microscopically phase-separated domains,[34] and we assume no significant deviations at the nanoscale. Therefore, the residence times inside the different nanoscopic domains yield values for the Ld phase of τ_{res} = (27 ± 3) μs and (30 ± 3) μs for 10 and 20 mol % Chol, respectively, and for the Lo phase of (158 ± 9) μs and (132 ± 14) μs for 10 and 20 mol % Chol, respectively. Although from our measurements we cannot directly estimate the sizes of these nanoscopic domains, the large spread of the diffusion times observed for the two larger gap areas (1080 nm^2 and 2025 nm^2) indicates that these gap areas already probe different nanoscopic regions during our measurements. On the other hand, the spread on the diffusion times reduces for the smallest antennas (300 nm^2) and is similar to the variations obtained from the fabrication procedure (Figure 5c). Reduced variations in the diffusion times imply that the sizes of the nanoscopic domains become comparable to the illumination area, which for the smallest antennas is 10 nm in size.

Overall, our results provide compelling evidence for the existence of nanoscopic domains in both the Ld and Lo phases of multicomponent lipid bilayers, with sizes around 10 nm and short transient residence times around 30 μs for the Ld and 150 μs for the Lo phases (Figure 5d). Nanoscopic domains in the Lo phase have also been recently detected by high-speed single particle tracking reporting on sizes and residence times that agree remarkably well to the values reported in this work using a completely different technique and experimental approach.[20] Interestingly, earlier stochastic models predicted that lipid rafts in living cells would have to be small (≤14 nm) with an average residence time of ∼60 μs in order to facilitate intermolecular collisions between different proteins.[21] These values come very close to our experimentally measured values. Moreover, molecular dynamics simulations of lipid diffusion within rafts and nonraft domains have predicted the existence of transient clusters with sizes around 10 nm and lifetimes in the microsecond range,[41] once more in excellent agreement with our experimental values. Thus, although the plasma membrane of living cells has a much higher complexity than our model lipid bilayers, we propose that the nanoscopic and highly transient domains detected in this model system might exhibit similar biophysical properties as those predicted in living cells.

Strikingly, our results show also the occurrence of nanoscopic domains in the Ld phase, which to our knowledge have not been detected before. However, there are ample experimental data that support their existence. Indeed, earlier FRET measurements showed heterogeneities in the Ld phase that depended on the amount of cholesterol and persisted even at physiological temperatures, hinting toward the existence of nanoscale domains in the Ld phase.[42,43] Moreover, recent d-NMR experiments showed a relatively large percentage of saturated lipids (17%) and Chol (20%) in the Ld phase, which is supposedly composed by only DOPC.[19] The presence of SM and Chol will lead to nanoscopic phase separation within the Ld phase with sizes and lifetimes that would most probably depend on the amount of Chol and SM.[42,43] In our experiments, we find that these nanoscopic domains are extremely short-lived with residence times below 30 μs, probably the reason why they have not been detected before. In fact, the temporal resolution of the high-speed SPT experiments reporting the presence of nanoscopic domains on the Lo phase was 20 μs, which is not enough to detect transient confinements around 30 μs.[20] By combining nanoscale observation areas, as provided by plasmonic antennas, with microsecond time resolution, as afforded by FCS, we have been able to resolve transient nanoscopic domains coexisting in both Ld and Lo phases of mimetic lipid membranes. It is worth mentioning that recent advancements in interferometric scattering (iSCAT) microscopy allow nowadays nanometer localization precision together with microsecond time resolution with the use of 20−40 nm gold beads as labeling probes.[20,39,44] Provided that careful controls on potential labeling artifacts and background characterization and removal are performed, iSCAT also constitutes an attractive tool to investigate dynamic processes on mimetic membranes at the nanometer scale.

CONCLUSIONS

In summary, we have exploited *in-plane* plasmonic nanogap antenna arrays to investigate the lateral organization of lipid model membranes at the nanoscale with microsecond time resolution. The suitability of *in-plane* antenna arrays has been validated on pure DOPC bilayers obtaining free diffusion over the length scales investigated (down to 10 nm), consistent with a homogeneous lipid distribution. Free diffusion was also observed on DOPC:SM binary mixtures, although a large spread of the diffusion times was retrieved indicating local fluctuations of SM within larger areas of solely DOPC, but without formation of detectable domains that would constrain dye diffusion. Addition of cholesterol resulted in microscopic phase separation and the formation of transient nanoscopic domains in both the Lo and Ld phases, with sizes below 10 nm and lifetimes in the microsecond time scale. Since the basic biochemistry operating in lipid model membranes is similar to the one in the plasma membrane, we propose that the nanoscopic domains detected here might correspond to the unstable lipid rafts predicted to exist in living cell membranes. The ultrahigh spatiotemporal resolution provided by *in-plane* plasmonic nanogap antennas holds great promise to unequivocally reveal their existence in living cells.

METHODS

Lipids. 1,2-dioleoyl-*sn*-glycero-3-phosphocholine (DOPC) and *N*-stearoyl-D-*erythro*-spingosylphosphorylcholine 18:0 (SM) were purchased from Avanti (Avanti Polar Lipids, Inc.). Cholesterol (Chol) ≥ 99% was purchased from Sigma-Aldrich and the fluorescent dye $DiIC_{18}(5)$ solid (DiD) from Molecular Probes, Life Technologies Corporation.

Fabrication of *in-Plane* Plasmonic Antenna Arrays. *In-plane* dimer antenna arrays with gaps of different sizes were fabricated in

DOI: 10.1021/acsnano.7b03177
ACS Nano 2017, 11, 7241−7250

gold onto glass-coverslips following a procedure described in ref 32. In brief, the antenna fabrication process was performed on a thin silicon nitride layer deposited on silicon substrates that provided suitable electrical conductivity and chemical stability for the subsequent process steps. Hydrogen-silsesquioxane (HSQ) resist was first spun and then patterned using electron beam lithography on top of the substrate. A thin layer of gold (50 nm thick) was then deposited by electron beam evaporation over the patterned HSQ structures, followed by a planarization step by flowable oxide spin coating. After etching back by Ar-based ion beam etching and removal of the remaining HSQ, the final antenna dimers were stripped from the substrates using a UV curable polymer. This step provided flipped over antennas with accessible gap regions onto optically transparent microscope coverslips. Prior to lipid bilayer deposition, the antenna substrates were carefully cleaned with ethanol, Milli-Q water rinsing, and UV light exposure for 1 min, followed by 3 min of ozone treatment.

Preparation of Lipid Model Membranes and Substrate Support. For the preparation of glass-supported lipid bilayers, glass coverslips were extensively cleaned with acetone, ethanol, ultrasonic bath, and in a UV/ozone cleaner with intermediate rinsing steps with pure Milli-Q water and immediately used afterward. Lipid mixtures of DOPC, DOPC:SM (1:1), and DOPC:SM:Chol (10/20 mol %) dissolved at 1 mg/mL in chloroform:methanol (9:1) together with 0.01 mol % of the fluorescent dye DiD were mixed in small glass bottles on ice at 4 °C and immediately deposited on the cleaned coverslips or antenna substrates. The gold antenna substrates were carefully cleaned with acetone, ethanol, and Milli-Q water, followed by a short UV/ozone plasma exposure (between 2 and 5 min) immediately prior to lipid bilayer deposition. The latter treatment removes any residual organic layer from the gold substrate, guaranteeing a chemically inert and hydrophilic surface.[40] All the steps were carried out under a fume hood. The different lipid mixtures were allowed to dry for roughly an hour in the presence of a weak nitrogen flow and then kept in vacuum for an additional hour. Consequently, the samples were hydrated in PBS (pH 7.4) and carefully rinsed to remove excess lipids. Samples were imaged and probed by FCS immediately after preparation. All measurements were performed at room temperature.

Estimation of the Illumination Areas for the Different Antenna Gaps. To estimate the illumination areas from our antenna gaps, we considered for the *x*-direction the mean values of the three gap sizes, as directly measured from TEM images (Supporting Information Figure S3), while for the *y*-direction, we took the distances corresponding to the full-width-at-half-maximum (fwhm) of the respective antenna excitation intensity profiles, as obtained from FDTD simulations (Supporting Information Figure S2b–d). The calculated gap areas are (288 ± 50) nm^2, (1080 ± 80) nm^2, and (2025 ± 110) nm^2 for the nominal 10, 30, and 45 nm gap sizes, respectively. The sizes of the illumination areas were further calibrated by measuring the diffusion times of the Alexa Fluor 647 dye in solution for five different antenna sizes (10, 25, 30, 35, and 45 nm) considering the reported diffusion coefficient of the dye (300 μm^2/s).[45] Results of the calibration are shown in the Supporting Information Figure S4. Excellent agreement between the calculated and calibrated values was obtained. For all the data reported, we used the calibrated values, which correspond to 300, 1080, and 2025 nm^2 for the nominal gap sizes of 10, 30, and 45 nm gap, respectively.

Fluorescence Microscopy and FCS. Fluorescence imaging and FCS measurements were performed using a commercial MicroTime 200 setup (PicoQuant). The excitation light of a linearly polarized picosecond laser diode (Pico-Quant LDH-D-C-640) operating at 640 nm in continuous wave mode was focused onto the sample through an Olympus UPLSAPO 60× , 1.2 NA water-immersion objective. A half-wave plate was used to control the polarization of the incoming light. The fluorescence signal was collected through the same objective, separated from the laser light by a dichroic mirror, split by a 50/50 beam splitter cube, and sent onto two avalanche photodiodes (APDs) (PicoQuant MPD- 50CT) after passing through a 30 μm pinhole conjugated to the focus plane. Two long-pass 650 nm filters were placed in front of the detectors in order to reject backscattered laser light and maximize the fluorescence signal collection. We used two APDs and performed cross-correlation between the two channels instead of autocorrelation of one channel, since it reduces artifacts due to the dead time of each detector and after pulses. A three-axis piezoelectric stage and controller (Physik Instrumente, Karlsruhe, Germany) allowed to scan the sample and precisely position the focus on individual nanoantennas.

FCS measurements were performed by illuminating the sample at an excitation power density of ~2 kW/cm^2. The commercial software package SymPhoTime 64 (PicoQuant) was used for the overall handling of the experiment, detection of fluorescent counts, computation of the autocorrelation curves $G(\tau)$, and fitting routines for the FCS analysis. The setup was calibrated by measuring the known three-dimensional diffusion coefficient of Alexa Fluor 647 in solution. Fluorescence time traces on individual nanoantennas were recorded for either 30 or 60 s, with a temporal resolution of 4 ps. $G(\tau)$ curves were generated over time windows of typically 10 s in length.

The calculated correlation curves $G(\tau)$ were fitted using a two-dimensional Brownian diffusion model, assuming a Gaussian beam profile as shown in eq 1:

$$G(\tau) = \sum_{i=0}^{n_{\mathrm{diff}}-1} \frac{A_i}{1 + \left(\frac{\tau}{\tau_i}\right)} \tag{1}$$

where n_{diff} is the number of independently diffusing species ($n_{\mathrm{diff}} = 2$ for the two-component fit used here) and A_i is the amplitude of the contribution of the i^{th} diffusing species with the corresponding diffusion time τ_i. We used a two-component fitting since excitation of the dimer antenna inside the nanoaperture leads to two distinct diffusion times as explained in ref 27. The shortest diffusion time corresponds to direct excitation at the antenna gap, while the second component corresponds to the diffusion times of molecules inside the nanoaperture but away from the antenna hotspot region. These molecules contribute weakly to the overall correlation curve since they are only excited by the residual light inside the nanoaperture (see also Supporting Information Figure S5 and Table S2). We also attempted to fit the curves using a three-component fitting, but in general the amplitude weight of the third component was either very small (below 3%) and/or rendered a fitting error.

ASSOCIATED CONTENT

Supporting Information

The Supporting Information is available free of charge on the ACS Publications website at DOI: 10.1021/acsnano.7b03177.

Experimental quality assessment of the four different model lipid bilayers by confocal excitation; *in-plane* antenna arrays and FDTD simulations; antenna gap size distribution measured from transmission electron microscopy (TEM) images; calibration measurements on AlexaFluor 647 in solution to assess the illumination areas of the antenna gaps; fluorescence intensity time traces and ACF curves for DOPC obtained upon parallel and perpendicularly polarized excitation of the antennas; FCS diffusion plots for the two ternary lipid mixtures at 10 and 20 mol % Chol; diffusion coefficients of DiD for the different lipid model membrane mixtures as obtained from confocal measurements; fitting values of the ACF curves for DOPC bilayers at different antenna gap areas (PDF)

AUTHOR INFORMATION

Corresponding Authors

*E-mail: maria.garcia-parajo@icfo.eu.
*E-mail: jerome.wenger@Fresnel.fr.

DOI: 10.1021/acsnano.7b03177
ACS Nano 2017, 11, 7241–7250

ORCID

Pamina M. Winkler: 0000-0002-4275-3639
Valentin Flauraud: 0000-0002-1393-3198
Jürgen Brugger: 0000-0002-7710-5930
Jérôme Wenger: 0000-0002-2145-5341
María F. García-Parajo: 0000-0001-6618-3944

Notes

The authors declare no competing financial interest.

ACKNOWLEDGMENTS

We thank K. J. E. Borgman and F. Campelo for fruitful discussions. The research leading to these results received funding from the European Commission's Seventh Framework Programme (FP7-ICT-2011-7) under grant agreements ERC StG 278242 (ExtendFRET), 288263 (NanoVista), Spanish Ministry of Economy and Competitiveness ("Severo Ochoa" Programme for Centres of Excellence in R&D (SEV-2015-0522) and FIS2014-56107-R), Fundació CELLEX (Barcelona), and CERCA Programme/Generalitat de Catalunya. P.M.W. is supported by the ICFOstepstone Fellowship, a COFUND Doctoral Programme of the Marie-Sklodowska-Curie-Action of the European Commission. R.R. is supported by the Erasmus Mundus Doctorate Program Europhotonics (grant 159224-1-2009-1-FR-ERA MUNDUS-EMJD).

REFERENCES

(1) Simons, K.; Ikonen, E. Functional Rafts in Cell Membranes. *Nature* **1997**, *387*, 569.
(2) Brown, D. A.; London, E. Functions of Lipid Rafts in Biological Membranes. *Annu. Rev. Cell Dev. Biol.* **1998**, *14*, 111−136.
(3) Pike, L. J. Rafts Defined: A Report on the Keystone Symposium on Lipid Rafts and Cell Function. *J. Lipid Res.* **2006**, *47*, 1597−1598.
(4) Lingwood, D.; Simons, K. Lipid Rafts as a Membrane-Organizing Principle. *Science* **2010**, *327*, 46−50.
(5) Brown, D. A.; London, E. Structure and Function of Sphingolipid- and Cholesterol-Rich Membrane Rafts. *J. Biol. Chem.* **2000**, *275*, 17221−17224.
(6) Hancock, J. F. Lipid Rafts: Contentious Only from Simplistic Standpoints. *Nat. Rev. Mol. Cell Biol.* **2006**, *7*, 456−462.
(7) Lingwood, D.; Ries, J.; Schwille, P.; Simons, K. Plasma Membranes Are Poised for Activation of Raft Phase Coalescence at Physiological Temperature. *Proc. Natl. Acad. Sci. U. S. A.* **2008**, *105*, 10005−10010.
(8) Mayor, S.; Rao, M. Rafts: Scale-Dependent, Active Lipid Organization at the Cell Surface: Raft Hypothesis. *Traffic* **2004**, *5*, 231−240.
(9) Eggeling, C.; Ringemann, C.; Medda, R.; Schwarzmann, G.; Sandhoff, K.; Polyakova, S.; Belov, V. N.; Hein, B.; Von Middendorff, C.; Schoenle, A.; Hell, S. W. Direct Observation of the Nanoscale Dynamics of Membrane Lipids in a Living Cell. *Nature* **2009**, *457*, 1159−1162.
(10) Simons, K.; Gerl, M. J. Revitalizing Membrane Rafts: New Tools and Insights. *Nat. Rev. Mol. Cell Biol.* **2010**, *11*, 688−699.
(11) Owen, D. M.; Williamson, D. J.; Magenau, A.; Gaus, K. Sub-Resolution Lipid Domains Exist in the Plasma Membrane and Regulate Protein Diffusion and Distribution. *Nat. Commun.* **2012**, *3*, 1256.
(12) Honigmann, A.; Mueller, V.; Ta, H.; Schoenle, A.; Sezgin, E.; Hell, S. W.; Eggeling, C. Scanning STED-FCS Reveals Spatiotemporal Heterogeneity of Lipid Interaction in the Plasma Membrane of Living Cells. *Nat. Commun.* **2014**, *5*, 5412.
(13) Vicidomini, G.; Ta, H.; Honigmann, A.; Mueller, V.; Clausen, M. P.; Waithe, D.; Galiani, S.; Sezgin, E.; Diaspro, A.; Hell, S. W.; Eggeling, C. STED-FLCS: An Advanced Tool to Reveal Spatiotemporal Heterogeneity of Molecular Membrane Dynamics. *Nano Lett.* **2015**, *15*, 5912−5918.
(14) Simons, K.; Toomre, D. Lipid Rafts and Signal Transduction. *Nat. Rev. Mol. Cell Biol.* **2000**, *1*, 31−39.
(15) Garcia-Parajo, M. F.; Cambi, A.; Torreno-Pina, J. A.; Thompson, N.; Jacobson, K. Nanoclustering as a Dominant Feature of Plasma Membrane Organization. *J. Cell Sci.* **2014**, *127*, 4995−5005.
(16) Dietrich, C.; Bagatolli, L. A.; Volovyk, Z. N.; Thompson, N. L.; Levi, M.; Jacobson, K.; Gratton, E. Lipid Rafts Reconstituted in Model Membranes. *Biophys. J.* **2001**, *80*, 1417−1428.
(17) Veatch, S. L.; Keller, S. L. Organization in Lipid Membranes Containing Cholesterol. *Phys. Rev. Lett.* **2002**, *89*, 268101.
(18) Chiantia, S.; Ries, J.; Kahya, N.; Schwille, P. Combined AFM and Two-Focus SFCS Study of Raft-Exhibiting Model Membranes. *ChemPhysChem* **2006**, *7*, 2409−2418.
(19) Yasuda, T.; Tsuchikawa, H.; Murata, M.; Matsumori, N. Deuterium NMR of Raft Model Membranes Reveals Domain-Specific Order Profiles and Compositional Distribution. *Biophys. J.* **2015**, *108*, 2502−2506.
(20) Wu, H.-M.; Lin, Y.-H.; Yen, T.-C.; Hsieh, C.-L. Nanoscopic Substructures of Raft-Mimetic Liquid-Ordered Membrane Domains Revealed by High-Speed Single-Particle Tracking. *Sci. Rep.* **2016**, *6*, 20542.
(21) Nicolau, D. V.; Burrage, K.; Parton, R. G.; Hancock, J. F. Identifying Optimal Lipid Raft Characteristics Required to Promote Nanoscale Protein-Protein Interactions on the Plasma Membrane. *Mol. Cell. Biol.* **2006**, *26*, 313−323.
(22) Honigmann, A.; Mueller, V.; Hell, S. W.; Eggeling, C. STED Microscopy Detects and Quantifies Liquid Phase Separation in Lipid Membranes Using a New Far-Red Emitting Fluorescent Phosphoglycerolipid Analogue. *Faraday Discuss.* **2013**, *161*, 77−89.
(23) Muehlschlegel, P.; Eisler, H.-J.; Martin, O. J. F.; Hecht, B.; Pohl, D. W. Resonant Optical Antennas. *Science* **2005**, *308*, 1607−1609.
(24) Schuck, P. J.; Fromm, D. P.; Sundaramurthy, A.; Kino, G. S.; Moerner, W. E. Improving the Mismatch between Light and Nanoscale Objects with Gold Bowtie Nanoantennas. *Phys. Rev. Lett.* **2005**, *94*, 017402.
(25) Kinkhabwala, A.; Yu, Z.; Fan, S.; Avlasevich, Y.; Muellen, K.; Moerner, W. E. Large Single-Molecule Fluorescence Enhancements Produced by a Bowtie Nanoantenna. *Nat. Photonics* **2009**, *3*, 654−657.
(26) Novotny, L.; Van Hulst, N. Antennas for Light. *Nat. Photonics* **2011**, *5*, 83−90.
(27) Punj, D.; Mivelle, M.; Moparthi, S. B.; Van Zanten, T. S.; Rigneault, H.; van Hulst, N. F.; Garcia-Parajo, M. F.; Wenger, J. A Plasmonic "Antenna-in-Box" Platform for Enhanced Single-Molecule Analysis at Micromolar Concentrations. *Nat. Nanotechnol.* **2013**, *8*, 512−516.
(28) Flauraud, V.; Van Zanten, T. S.; Mivelle, M.; Manzo, C.; Garcia Parajo, M. F.; Brugger, J. Large-Scale Arrays of Bowtie Nanoaperture Antennas for Nanoscale Dynamics in Living Cell Membranes. *Nano Lett.* **2015**, *15*, 4176−4182.
(29) Holzmeister, P.; Acuna, G. P.; Grohmann, D.; Tinnefeld, P. Breaking the Concentration Limit of Optical Single-Molecule Detection. *Chem. Soc. Rev.* **2014**, *43*, 1014−1028.
(30) Puchkova, A.; Vietz, C.; Pibiri, E.; Wuensch, B.; Sanz Paz, M.; Acuna, G. P.; Tinnefeld, P. DNA Origami Nanoantennas with over 5000-Fold Fluorescence Enhancement and Single-Molecule Detection at 25 μM. *Nano Lett.* **2015**, *15*, 8354−8359.
(31) Pradhan, B.; Khatua, S.; Gupta, A.; Aartsma, T.; Canters, G.; Orrit, M. Gold-Nanorod-Enhanced Fluorescence Correlation Spectroscopy of Fluorophores with High Quantum Yield in Lipid Bilayers. *J. Phys. Chem. C* **2016**, *120*, 25996−26003.
(32) Flauraud, V.; Regmi, R.; Winkler, P. M.; Alexander, D. T. L.; Rigneault, H.; Van Hulst, N. F.; García-Parajo, M. F.; Wenger, J.; Brugger, J. *In-Plane* Plasmonic Antenna Arrays with Surface Nanogaps for Giant Fluorescence Enhancement. *Nano Lett.* **2017**, *17*, 1703−1710.
(33) Chiantia, S.; Kahya, N.; Schwille, P. Dehydration Damage of Domain-Exhibiting Supported Bilayers: An AFM Study on the Protective Effects of Disaccharides and Other Stabilizing Substances. *Langmuir* **2005**, *21*, 6317−6323.

DOI: 10.1021/acsnano.7b03177
ACS Nano 2017, 11, 7241−7250

(34) Kahya, N.; Scherfeld, D.; Bacia, K.; Poolman, B.; Schwille, P. Probing Lipid Mobility of Raft-Exhibiting Model Membranes by Fluorescence Correlation Spectroscopy. *J. Biol. Chem.* **2003**, *278*, 28109−28115.
(35) Sezgin, E.; Levental, I.; Grzybek, M.; Schwarzmann, G.; Mueller, V.; Honigmann, A.; Belov, V. N.; Eggeling, C.; Coskun, Ue.; Simons, K.; Schwille, P. Partitioning, Diffusion, and Ligand Binding of Raft Lipid Analogs in Model and Cellular Plasma Membranes. *Biochim. Biophys. Acta, Biomembr.* **2012**, *1818*, 1777−1784.
(36) Wawrezinieck, L.; Rigneault, H.; Marguet, D.; Lenne, P.-F. Fluorescence Correlation Spectroscopy Diffusion Laws to Probe the Submicron Cell Membrane Organization. *Biophys. J.* **2005**, *89*, 4029−4042.
(37) Favard, C.; Wenger, J.; Lenne, P.-F.; Rigneault, H. FCS Diffusion Laws in Two-Phase Lipid Membranes: Determination of Domain Mean Size by Experiments and Monte Carlo Simulations. *Biophys. J.* **2011**, *100*, 1242−1251.
(38) Baffou, G.; Quidant, R.; García De Abajo, F. J. Nanoscale Control of Optical Heating in Complex Plasmonic Systems. *ACS Nano* **2010**, *4*, 709−716.
(39) Spillane, K. M.; Ortega-Arroyo, J.; De Wit, G.; Eggeling, C.; Ewers, H.; Wallace, M. I.; Kukura, P. High-Speed Single-Particle Tracking of GM1 in Model Membranes Reveals Anomalous Diffusion Due to Interleaflet Coupling and Molecular Pinning. *Nano Lett.* **2014**, *14*, 5390−5397.
(40) Worley, C. G.; Linton, R. W. Removing Sulfur from Gold Using Ultraviolet/Ozone Cleaning. *J. Vac. Sci. Technol., A* **1995**, *13*, 2281−2284.
(41) Apajalahti, T.; Niemela, P.; Govindan, P. N.; Miettinen, M. S.; Salonen, E.; Marrink, S.-J.; Vattulainen, I. Concerted Diffusion of Lipids in Raft-Like Membranes. *Faraday Discuss.* **2010**, *144*, 411−430.
(42) Silvius, J. R. Fluorescence Energy Transfer Reveals Microdomain Formation at Physiological Temperatures in Lipid Mixtures Modeling the Outer Leaflet of the Plasma Membrane. *Biophys. J.* **2003**, *85*, 1034−1045.
(43) De Almeida, R. F. M.; Loura, L. M. S.; Fedorov, A.; Prieto, M. Lipid Rafts Have Different Sizes Depending on Membrane Composition: A Time-Resolved Fluorescence Resonance Energy Transfer Study. *J. Mol. Biol.* **2005**, *346*, 1109−1120.
(44) Spindler, S.; Ehrig, J.; Koenig, K.; Nowak, T.; Piliarik, M.; Stein, H. E.; Taylor, R. W.; Garanger, E.; Lecommandoux, S.; Alves, I. D.; Sandoghdar, V. Visualization of Lipids and Proteins at High Spatial and Temporal Resolution *via* Interferometric Scattering (iSCAT) Microscopy. *J. Phys. D: Appl. Phys.* **2016**, *49*, 274002.
(45) Kapusta, P. *Absolute Diffusion Coefficients: Compilation of Reference Data for FCS Calibration*. http://www.picoquant.com/images/uploads/page/files/7353/appnote_diffusioncoefficients.pdf (accessed June 29, 2017).

DOI: 10.1021/acsnano.7b03177
ACS Nano 2017, 11, 7241−7250